PHILOSOPHICAL TRANSACTIONS OF THE ROYAL SOCIETY A MATHEMATICAL, PHYSICAL & ENGINEERING SCIENCES

Geomagnetic palaeointensities and astrochronological ages for the Matuyama – Brunhes boundary and the boundaries of the Jaramillo Subchron: palaeomagnetic and oxygen isotope records from ODP Site 983

J. E. T. Channell and H. F. Kleiven

Phil. Trans. R. Soc. Lond. A 2000 **358**, 1027-1047
doi: 10.1098/rsta.2000.0572

THE ROYAL SOCIETY

Geomagnetic palaeointensities and astrochronological ages for the Matuyama–Brunhes boundary and the boundaries of the Jaramillo Subchron: palaeomagnetic and oxygen isotope records from ODP Site 983

By J. E. T. Channell[1] and H. F. Kleiven[2]

[1] *Department of Geological Sciences, University of Florida, PO Box 112120, Gainesville, FL 32611-2120, USA*

[2] *Department of Geology, University of Bergen, N-5007 Bergen, Norway*

We have measured relative geomagnetic palaeointensity proxies, palaeomagnetic directions, and δ^{18}O for the 700–1100 ka interval from ODP Site 983 (Gardar Drift, North Atlantic), where mean sedimentation rates are *ca.* 13 cm kyr^{-1}. The age model was generated by matching the benthic δ^{18}O data to the Ice Volume Model and confirmed by tuning the precessional components of both signals. For the Matuyama–Brunhes boundary (MBB) and the boundaries of the Jaramillo Subchronozone, the duration of the polarity reversal process, defined by virtual geomagnetic polar latitudes of less than 45°, is *ca.* 5 kyr. Whereas the generally accepted astrochronological estimates for the boundaries of the Jaramillo Subchronozone lie within the polarity transitions as recorded at Site 983, the astrochronological age for the Matuyama–Brunhes polarity transition (780 ka) is *ca.* 5 kyr older than the onset of this transition at Site 983 (775 ka). The polarity reversals lie within palaeointensity lows, with abrupt recovery of palaeointensity post reversal. There is no progressive ('saw-tooth') decrease in palaeointensity within the Jaramillo Subchronozone or between the top of the Jaramillo and the MBB, but rather, within polarity chrons, several short intervals of low palaeointensity which sometimes coincide with high-amplitude secular variation. Orbital (100 and 41 kyr) periods are present in the palaeointensity record. As they are not obviously attributable to climate/lithology in these records, they may be a feature of the geomagnetic field itself.

Keywords: geomagnetic secular variation; geomagnetic palaeointensity; Matuyama–Brunhes boundary; Jaramillo Subchron; ODP Site 983; Iceland Basin

1. Introduction

Ocean Drilling Program (ODP) Site 983 (60.40° N, 336.36° E, 1983 m water depth), located close to the crest of the Gardar Drift south of Iceland (figure 1), was drilled in late July 1995. The three holes drilled at the site provided a complete composite section to the base of the Olduvai Subchronozone (Shipboard Scientific Party 1996).

Deposition in the Gardar Drift has been driven by thermohaline circulation associated with Norwegian Sea Overflow Water (NSOW) spilling over the Iceland–Scotland Ridge. Accumulation rates have been enhanced by horizontal advection of fine material suspended in the nepheloid layer (Wold 1994; McCave & Tucholke 1986). The Gardar Drift accumulated throughout the Pleistocene at rates of 5–20 cm kyr^{-1}, and provides one of the most detailed Pleistocene climatic records retrieved from the North Atlantic. The composite section was generated shipboard using magnetic susceptibility, GRAPE density and reflectance data from the measurement systems track (MST) to correlate the three holes and splice together an optimal (complete and undisturbed) record of the sedimentary sequence (see Hagelberg *et al*. (1992) for review of methods). A preliminary magnetic polarity stratigraphy was generated on the 'archive' halves of core sections from each hole, using the shipboard pass-through magnetometer (Shipboard Scientific Party 1996) after demagnetization at a single peak alternating field (usually 25 mT). The high rate of core recovery and the need to avoid processing bottlenecks necessitated this abbreviated demagnetization treatment. Subsequent shorebased treatment of 7 cm^3 discrete samples, collected shipboard in plastic cubes, served to ground-truth the shipboard magnetic stratigraphy (Channell & Lehman 1999).

Here we report the magnetic properties and $\delta^{18}O$ of the 700–1100 ka interval at Site 983. The objective is to place the palaeomagnetic directional and palaeointensity records on a firm isotopic age model in order to document the behaviour of the geomagnetic field during the 400 kyr interval which includes the Matuyama–Brunhes boundary (MBB) and the Jaramillo Subchron.

2. Oxygen isotope stratigraphy

The interval from 700 to 1200 ka was sampled continuously (nominally at 2 cm intervals) for stable isotopic analyses of benthic and planktic foraminifera. The benthic foraminiferal isotopic analyses were performed on the taxon *Cibicidoides*, principally made up of *C. wuellerstorfi*. The planktic foraminiferal isotopic analyses were performed on *Neogloboquadrina pachyderma* (sinistral). Both species were selected from the >150 μm size fraction. The abundance of *N. pachyderma* (sinistral) allowed the planktic record to be acquired at a 2–5 cm (*ca.* 500 year) resolution, whereas the spacing of the benthic $\delta^{18}O$ is 10 cm or greater due to the relative scarcity of *Cibicidoides* spp.

Stable isotope measurements of *N. pachyderma* (s.) specimens were made at the University of Bergen on a Finnigan MAT251 coupled to an automated carbonate preparation device, whereas the isotope measurements of *Cibicidoides* spp. were carried out with a VG Isogas PRISM mass spectrometer at the University of Florida. A small number of benthic stable isotope measurements were made at Scripps Institution of Oceanography on a Finnigan MAT252 and at the University of Cambridge on a VG Isogas PRISM. Isotope data from all these laboratories were calibrated using the NIST (NBS) 19 standard, and values are reported relative to PDB.

Oxygen isotopic stages 18–35 can easily be identified in the Site 983 benthic record by matching to other deep-sea sediment $\delta^{18}O$ records (figure 2). Orbital variability in $\delta^{18}O$ is clearly present in the Site 983 record, indicating that Milankovitch forced ice-volume changes are controlling the large-scale fluctuations. Mean sedimentation rates at Site 983 are three times higher than at Site 677 (13 cm kyr^{-1} versus 4 cm kyr^{-1}).

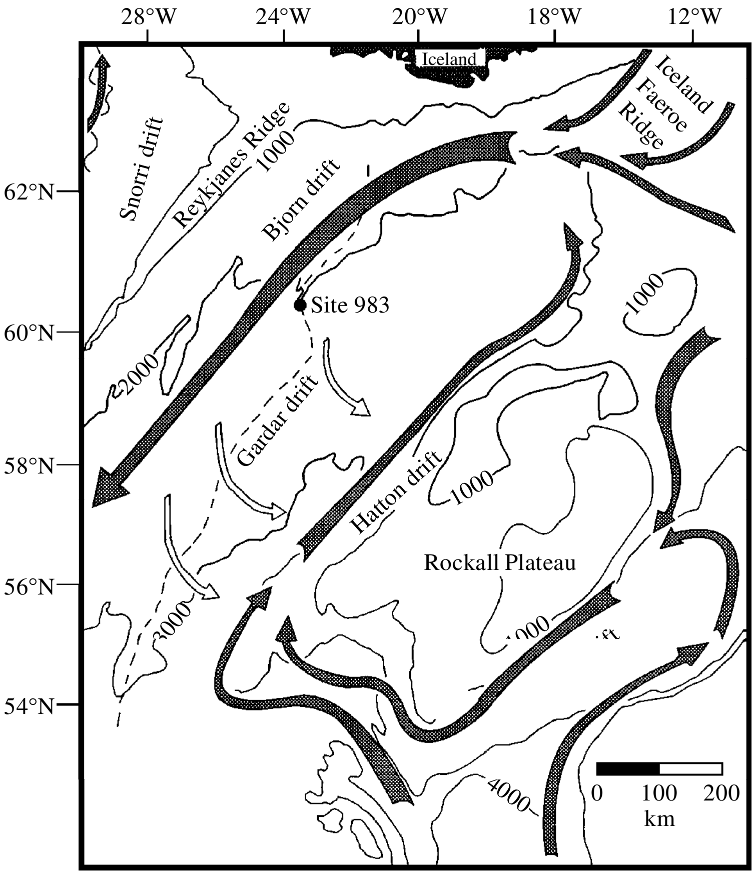

Figure 1. Map showing the location of ODP Site 983 at 60°24′ N, 23°38′ S and 1983 m water depth. Site 983 is located near the head of the Gardar Drift which extends to the south-southwest, following the path of deep overflow currents (Norwegian Sea Overflow Water, NSOW, as shown by arrows) from the Iceland–Faeroe Ridge. Dashed line shows crest of Gardar Drift. Map after Manley & Caress (1994) and McCave *et al*. (1980). Bathymetry in metres.

When compared with other records (figure 2), many additional isotope events indicating sub-orbital variability are well defined in the Site 983 record.

Within isotopic stage 18, we observe supplementary peaks both in the planktic and benthic records (figure 3*a*) which have previously been observed only in the planktic record of core MD900963 (figure 2), where they were interpreted to be related to precession (Bassinot *et al*. 1994). The stage 19–18 transition displays a succession of light δ^{18}O peaks superimposed on the trend towards glacial values. These parallel, sub-orbital oscillations of the planktic and benthic records imply that the isotopic signal was rapidly transferred from surface water to depth; indicating that surface and deep waters were strongly coupled, perhaps as a result of rapid waxing and waning of ice sheets in the near surroundings accompanied by glacial meltwater fluxes. Similar shorter-period fluctuations occur in the stage 21–20 transition, and there are also excursions in δ^{18}O near the stage 25–24, 31–30 and 35–34 transitions.

Isotope stage 21 stands out as an interglacial abruptly interrupted by cool periods

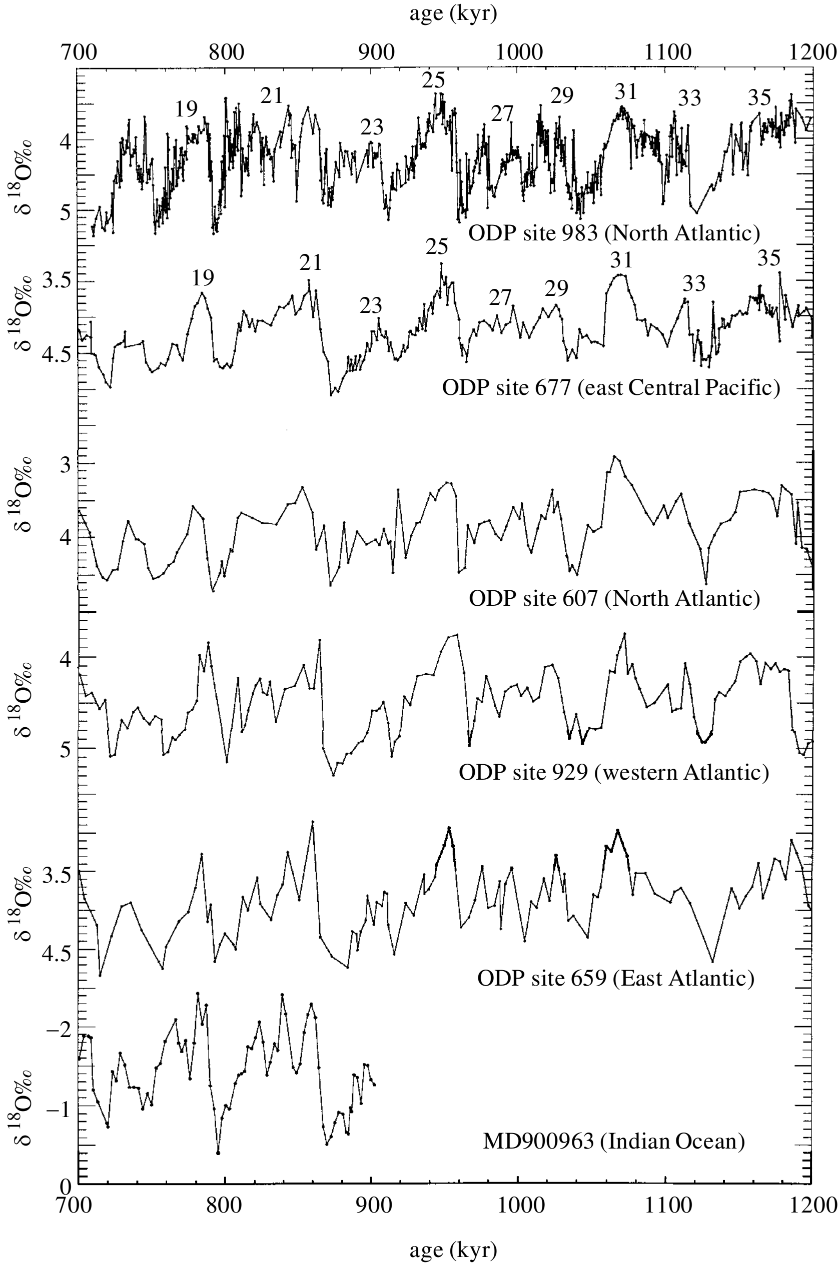

Figure 2. Benthic δ^{18}O records for isotopic stages 18–35 (700–1200 ka): Ocean Drilling Program Site 983 (this paper), ODP Site 677 (Shackleton *et al.* 1990), ODP Site 607 (Ruddiman *et al.* 1989), ODP Site 929 (Bickert *et al.* 1997), ODP Site 659 (Tiedemann *et al.* 1994), and the planktic δ^{18}O record from MD900963 (Bassinot *et al.* 1994). Isotope stages are identified according to Shackleton *et al.* (1990) and this paper.

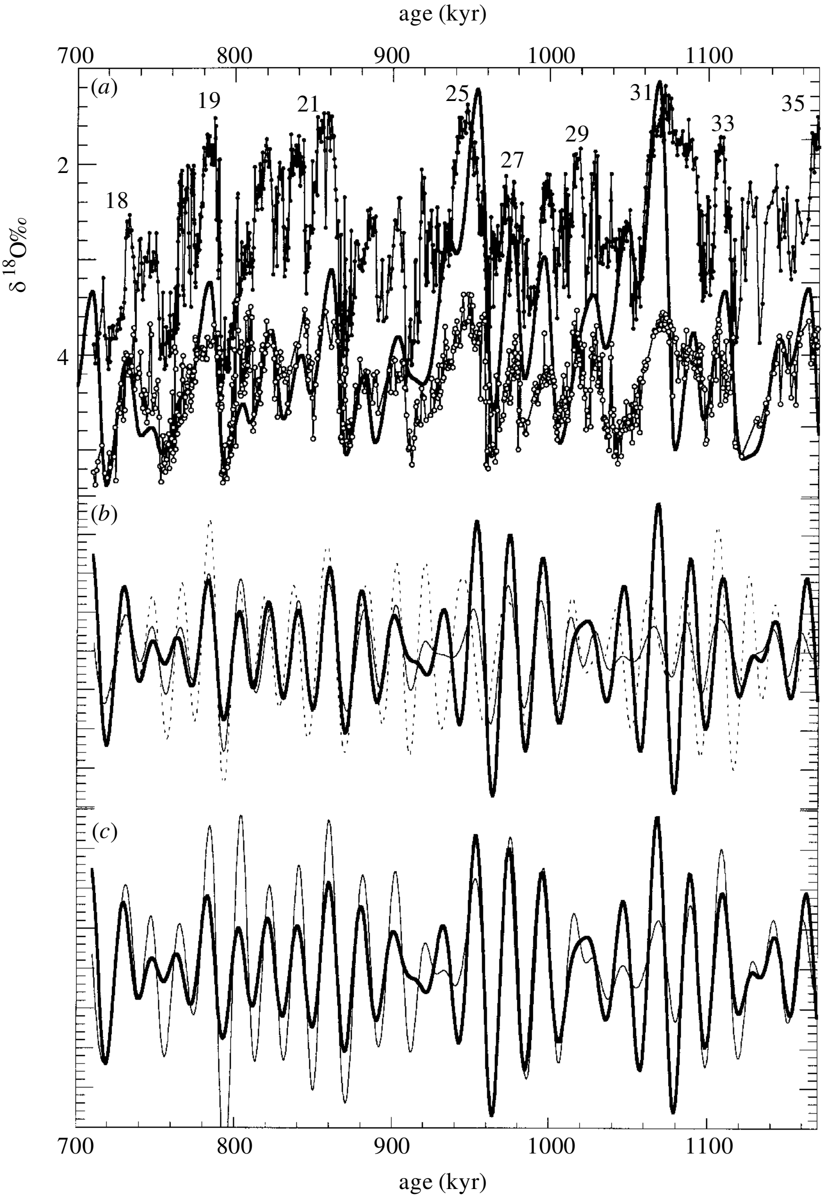

Figure 3. (*a*) Planktic (solid symbols) and benthic (open symbols) δ^{18}O records from ODP Site 983 compared with the Ice Volume Model (thick line) calculated after Imbrie & Imbrie (1980). (*b*) After initial fit of benthic δ^{18}O record to the Ice Volume Model: output of a Gaussian filter centred on 20 kyr (0.05 kyr^{-1}) with a 0.02 kyr^{-1} bandpass applied to the Ice Volume Model (thick line), benthic δ^{18}O record (thin line), and planktic δ^{18}O record (dashed line). (*c*) After tuning of the filtered (20 kyr) records in figure 2*b*: output of a Gaussian filter centred on 20 kyr (0.05 kyr^{-1}) with a 0.02 kyr^{-1} bandpass applied to the Ice Volume Model (thick line) and the benthic δ^{18}O record (thin line).

which define a precession-related tripartite stage 21. Isotope analyses from ODP Site 929 and MD900963 (figure 2) also suggest a partition of stage 21, but the Site 983 record exhibits significantly greater amplitude (1–0.5‰) and differs from other deep sea records, which generally show stage 21 as a warm and stable period. Also noteworthy is the interval between stages 26 and 30, where significant millennial scale variability is superimposed upon five light benthic δ^{18}O peaks (more than 1‰ amplitude), attributed to precession-related forcing. Such instability, with pacing indistinguishable from that of the last glacial cycle, appears to characterize all observed climate states during the Mid-Pleistocene interval, suggesting that sub-orbital variability has been a fundamental part of the climate system in the North Atlantic region. This view is supported by recent results from the Early Pleistocene (Raymo *et al*. 1998) and Late Pleistocene (McManus *et al*. 1999) in the North Atlantic region; implying that climatic instability on sub-orbital time-scales existed during glacial and interglacial intervals throughout the Pleistocene.

Notable differences between the Site 983 records and the other records spanning the Mid-Pleistocene interval (figure 2) can be attributed to the greater resolution of the Site 983 record. Local climatic processes taking place in the sub-polar North Atlantic are clearly superimposed on the global ice volume signal at Site 983. As mentioned above, some of these sub-orbital events could result from local processes transferring the highly negative δ^{18}O surface waters downward either through melt water injection or brine formation (Vidal *et al*. 1998; Dokken & Jansen 1999).

3. Age model

Site 983 provides the most detailed Mid-Pleistocene δ^{18}O record retrieved from the North Atlantic, and it allows us to compare in detail palaeoclimatic oscillations with variations in orbital forcing and thus test the accuracy of the orbitally derived time-scale of Shackleton *et al*. (1990). Figure 3*a* shows the planktic and benthic oxygen isotope records from Site 983 together with an ice volume simulation using the model of Imbrie & Imbrie (1980). We chose to use the latter as our tuning target, because it has proved to be a powerful target for the Late Pleistocene (Martinson *et al*. 1987; Bassinot *et al*. 1994) as well as for the Early Pleistocene (Shackleton *et al*. 1990). This model assumes that the rate of climate response (growth or decay of ice sheets) is proportional to the magnitude of summer insolation forcing at 65° N. We constructed this target curve (figure 3*a*) using the 65° N July insolation curve of Berger & Loutre (1991).

Our procedure was firstly to match the benthic δ^{18}O record from Site 983 to the target using linear interpolation between tie points (figure 3*a*). This procedure was fairly straightforward because the precession-related oscillations are well expressed in the δ^{18}O records from Site 983. When assigning the tie points, we gave the glacial–interglacial transitions higher priority than the centres of glacial or interglacial intervals. We assumed constant sedimentation rates between tie points, resulting in a change in sedimentation rate more or less abruptly at these control points (figure 4). This assumption may be realistic when the tie points correspond to glacial–interglacial transitions, when environmental changes might be expected to effect the sedimentation rates. Moreover, assigning tie points at high-amplitude transitions is probably more accurate than the designation of any particular peak or

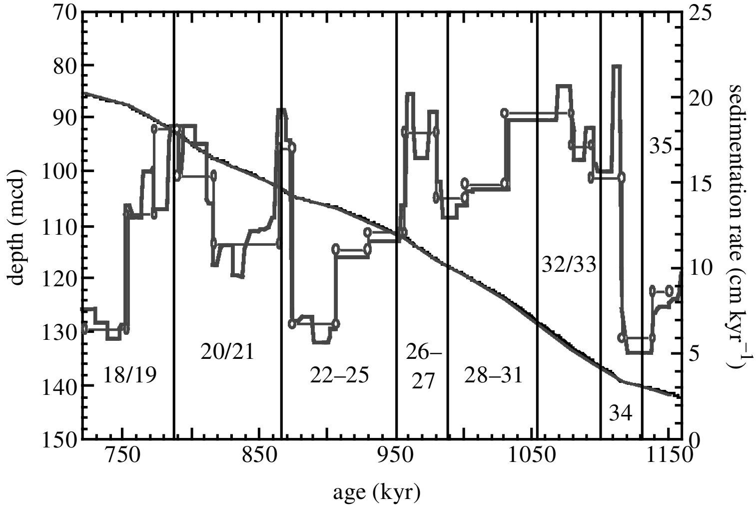

Figure 4. Age–depth map and interval sedimentation rates for the composite section at ODP Site 983. The thin line connecting open circles indicates interval sedimentation rates after initial fit of the benthic δ^{18}O record to the Ice Volume Model. The thick line represents the interval sedimentation rates after final tuning using the 20 kyr filter outputs (see text). The age–depth plots (continuous thin lines) are essentially identical before and after final tuning.

Table 1.

metres composite depth	age (ka)
85.58	722
87.56	753
90.18	773
93.25	790
97.4	817
102.89	865
104.59	875
106.74	907
109.29	930
112.54	957
116.65	980
119.6	1001
124.06	1031
133.18	1079
135.75	1094
139.25	1117
140.55	1139
141.67	1152

trough in intervals displaying considerable high-frequency, low-amplitude variability. Tie points for this initial age model are given in table 1.

Down to stage 22, the benthic δ^{18}O record and the ice volume curve are very similar, and a good match can be achieved interpreting stage 18 as containing two precession cycles and stage 21 as containing three precession cycles. When the extra peak in stage 23 is tuned to a precession oscillation and the double peaks of stage 29 are interpreted to be part of one precession cycle, the tuning down to stage 29 is a fairly obvious. Once the stage 29 is tuned, however, we need to assign a precession cycle to the transition between stages 29 and 30 in order keep pace with the Ice Volume Model. There is some ambiguity in this interval in the benthic δ^{18}O record, but the planktic δ^{18}O record can be matched with confidence to the Ice Volume Model. To respect the number of precession-related peaks in the Ice Volume Model, we assigned two precession cycles to the major δ^{18}O peak found in stage 31, and tuned stage 33 to the low ice volume peak at 1120 ka. As our isotope records do not extend beyond the peak of isotope stage 35, it was difficult to pick an end point for our tuning procedure. But, the close correlation between Site 983 and Site 677 (figure 2) (the latter also tuned to the Ice Volume Model) allowed this task to be completed, and we thus conclude that our record spans the time-interval from *ca.* 710 to 1170 ka.

This first step was followed by a fine-tuning of the extracted precession components of the benthic δ^{18}O record, to the precession component of the Ice Volume Model. The Ice Volume Model and the benthic (and planktic) δ^{18}O record were passed through a Gaussian filter centred on 20 kyr (0.05 kyr^{-1}) with a 0.02 kyr^{-1} bandwidth (figure 3*b*). The resulting match of filter-outputs led to a slight adjustment of the original match of the unfiltered benthic δ^{18}O to the Ice Volume Model. The resulting depth-age map (figure 4) indicates that sedimentation rates vary in a range from 5 to 22 cm kyr^{-1}, tending to be lower during glacial intervals. The Ice Volume Model and the final tuned benthic δ^{18}O record were then filtered again (figure 3*c*), and the match between the two filtered records are in good agreement, suggesting that an accurate tuning solution has been obtained.

4. Magnetic properties

Magnetic properties were largely determined from U-channel samples collected from the archive halves of the composite section. U-channels have a 2×2 cm^2 square cross-section, are up to 1.5 m in length, with a clip-on lid constituting one of the sides (Tauxe *et al.* 1983). Magnetic remanence of U-channels was measured at 1 cm intervals using the 2G Enterprises small-access pass-through magnetometers at Gif-sur-Yvette (France) and the University of Florida (see Weeks *et al.* 1993). The response functions of the three orthogonal magnetometer pick-up coils yield effective U-channel lengths in the sensing region of 4.2 cm for vertical and horizontal (X and Y) and 6.2 cm for the axial direction (Z). Hence, although measurements were made at 1 cm intervals downcore, there is an inherent smoothing in the measurement procedure. Volume magnetic susceptibility (κ) was measured on U-channels at 1 cm intervals using a 45 mm diameter loop. Natural remanent magnetization (NRM) was first measured in conjunction with stepwise alternating field (AF) demagnetization. Anhysteretic remanence (ARM) and then isothermal remanence (IRM) were imposed on the samples, and these remanences were progressively AF demagnetized. The ARM was acquired in a 100 mT alternating field with a 0.05 mT bias DC field, and the IRM was acquired in a 500 mT DC field. ARM and IRM values were used to normalize the NRM for variations in concentration of remanence carrying grains, and hence generate the palaeointensity proxies.

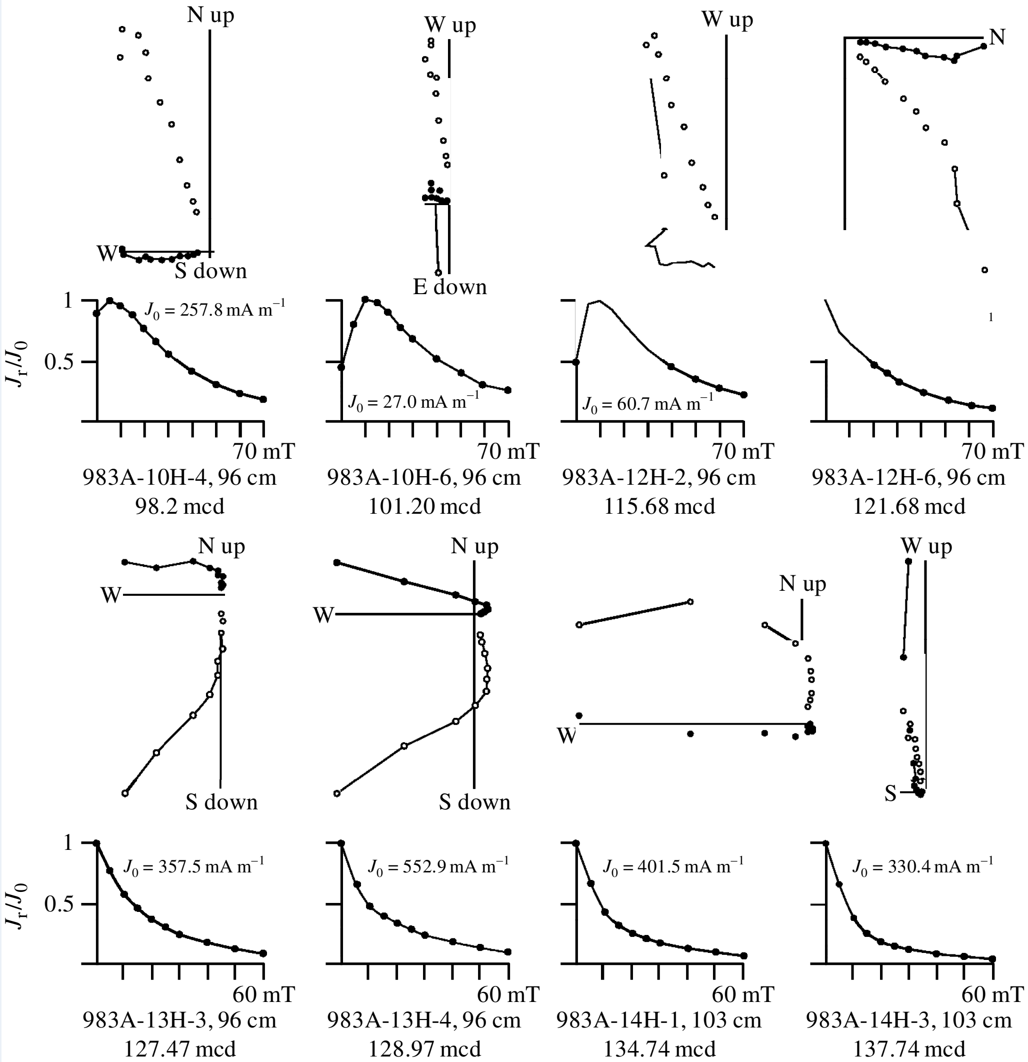

Figure 5. Orthogonal projection of alternating field demagnetization data for samples from Hole 983A. Open and solid symbols indicate projection on the vertical and horizontal planes, respectively. The NRM intensity before demagnetization (J_0) is indicated, and the peak demagnetization fields are indicated in mT. The hole, core, section and depth in section (cm), and the total depth in metres below the sediment–water interface (mcd) are indicated.

Orthogonal projections of AF demagnetization data indicate that the characteristic magnetization component is isolated at peak fields of 20–25 mT after removal of low coercivity component attributed to the drilling process (figure 5). About 10% of the remanence remain after demagnetization in peak fields of 70 mT and the median destructive field (20–30 mT) is consistent with magnetite as the principal remanence carrier. The plot of anhysteretic susceptibility against susceptibility (figure 6*a*) can be used to assess the uniformity in grain size of magnetite. The reasonably tight grouping along a line emanating from the origin of the plot (figure 6*a*) is consistent

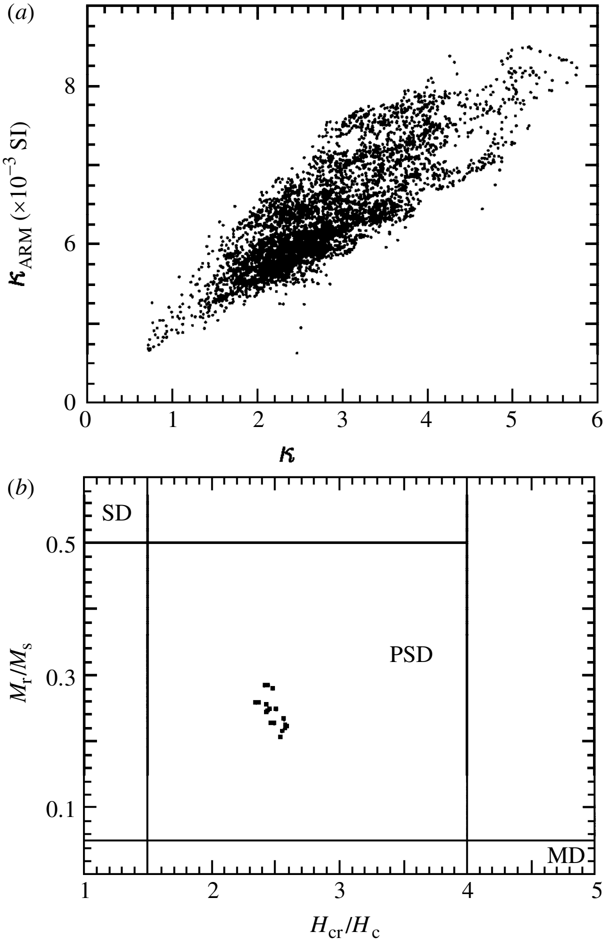

Figure 6. (*a*) Anhysteretic susceptibility ($\kappa_{\rm ARM}$) plotted against volume susceptibility (κ) for the late Matuyama composite section at Site 983, (*b*) hysteresis ratio plot for samples from the late Matuyama composite section at Site 983. M_r, saturation remanence; M_s, saturation magnetization; H_c, coercive force; H_{cr}, remanent coercivity; SD, single domain; PSD, pseudo-single domain; MD, multidomain (plot style after Day *et al.* (1977)).

with fairly uniform magnetite grain size in the 5–10 μm range (King *et al.* 1983). Hysteresis ratios lie in the pseudo-single domain (PSD) field (figure 6*b*) according to Day *et al.* (1977).

Volume magnetic susceptibility measured at 1 cm intervals along U-channel samples varies by a factor of about 5 (figure 7). The prominent warm isotopic stages (19, 21, 25 and 31) have relatively low susceptibility, due partly to dilution by calcium carbonate. IRM and ARM also vary by a factor of about 5, with a less pronounced correlation with the δ^{18}O record (figure 7). The magnetite grain size sensitive parameter ARM/κ (figure 7) varies in a narrow range (as expected from figure 6*a*) indicating no pronounced variations in magnetite grain size. The Brunhes Chronozone at Site 983 has very similar magnetic properties (see Channell *et al.* 1997, 1998) to those described here. It appears that the Brunhes and Late Matuyama Chronozones at Site

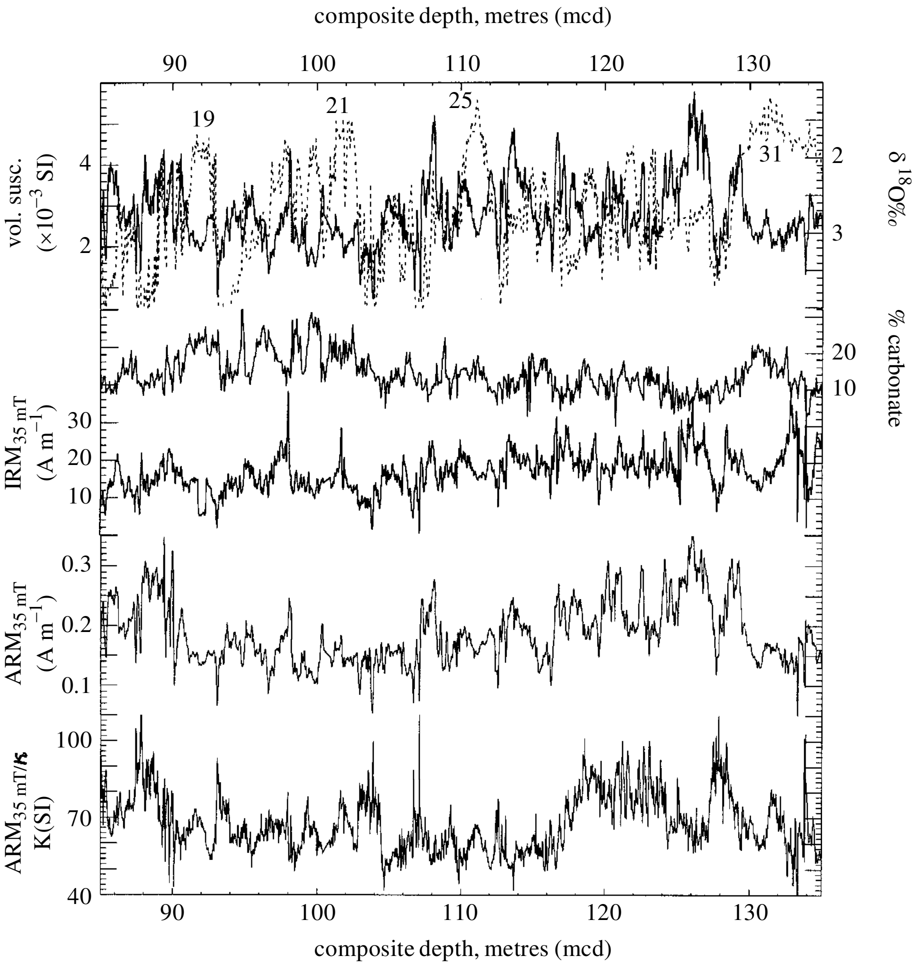

Figure 7. Site 983 magnetic data, planktic δ^{18}O record (dashed line) and percent carbonate data plotted against depth (mcd). IRM and ARM intensities are plotted after demagnetization at peak fields of 35 mT. Prominent interglacial stages are numbered on the δ^{18}O record. Percent carbonate after Ortiz *et al.* (1999).

983 are characterized by rather uniform magnetite grain size in the few micrometres (less than 10 µm) grain size range. Channell *et al.* (1998) used the thermal demagnetization of IRM to demonstrate the low levels of haematite in the Brunhes Chron at Site 983. The optimal conditions for palaeointensity determinations (see King *et al.* 1983; Tauxe 1993) are that fine-grained magnetite be the exclusive remanence carrier and that concentrations of these grains vary by no more than a factor of 10. These conditions appear to be satisfied in the Brunhes and late Matuyama chronozones at Site 983.

5. Magnetization component directions

The magnetic overprint attributed to the drilling process is removed at peak alternating fields of 20–25 mT (figure 5). The origin of this secondary component is not

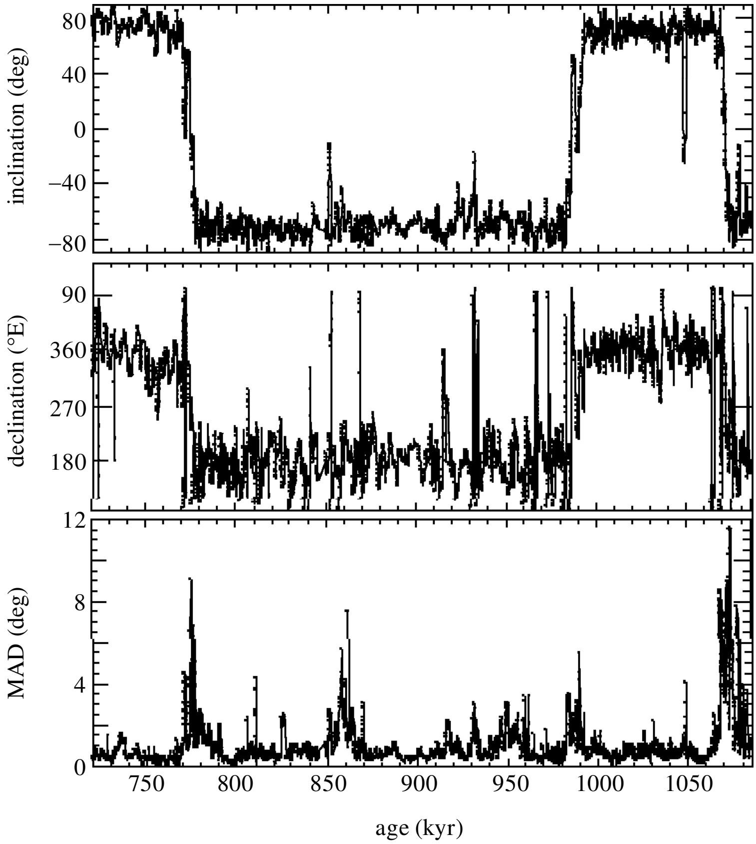

Figure 8. Component declinations and inclinations, and corresponding maximum angular deviation values, computed at 1 cm intervals and placed on the tuned isotope age model.

well understood. It is probably a viscous remanence (VRM) produced by magnetic fields within the drill string, possibly augmented by some sort of stirred remanence (StRM) produced by drilling disturbance. As mentioned above, archive halves of the composite section were demagnetized at peak fields of 25 mT to produce the shipboard polarity stratigraphy. In the stratigraphic interval discussed here, the NRMs of all U-channels collected from the archive halves of the composite section were stepwise demagnetized in peak fields of 25, 30, 35, 40, 45 and 60 mT. Further demagnetization steps were carried out for individual U-channels. In order to compute the characteristic magnetization component, the standard three-dimensional least-squares line-fitting routine (Kirschvink 1980) was applied each 1 cm downcore to the 25–60 mT demagnetization interval. The maximum angular deviation values are generally less than 10° (figure 8) indicating that the components are well defined in this demagnetization interval. The declinations and inclinations of the characteristic magnetization component indicate that the interval comprises the base of the Brunhes Chronozone to just below the Jaramillo Subchronozone (figure 8). Several intervals of high-amplitude secular variation are apparent in the top of the Matuyama Chronozone and within the Jaramillo Subchronozone. The mean inclination (74°) coincides with the expected mean inclination at the sampling site.

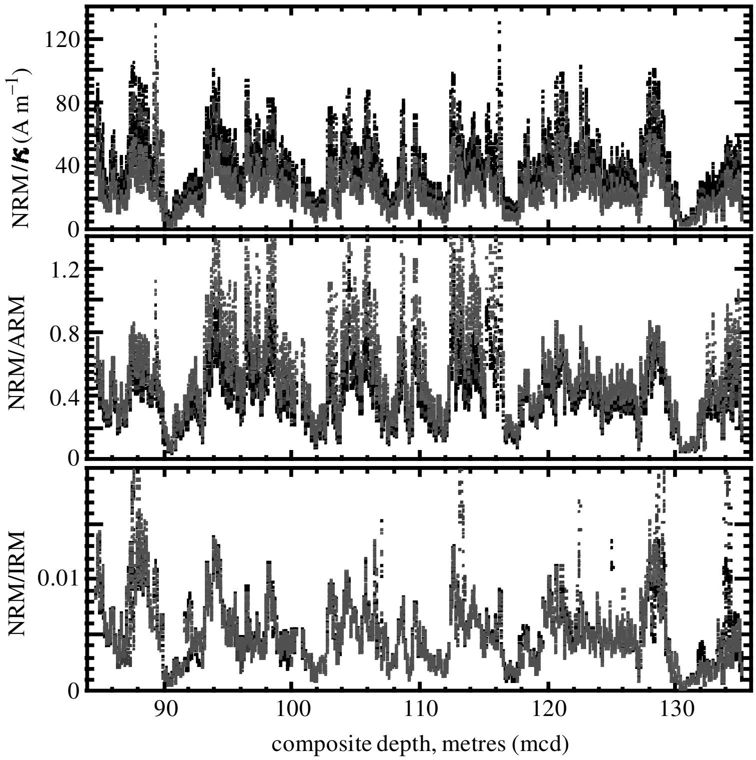

Figure 9. NRM/κ after demagnetization (of NRM) at peak fields in the 25–45 mT range, NRM/ARM after demagnetization (of both remanences) at peak fields in the 25–45 mT range, and NRM/IRM after demagnetization (of both remanences) at peak fields in the 25–45 mT range.

6. Palaeointensity estimates

Palaeointensity proxies are constructed by normalizing the NRM intensity by a parameter (such as κ, ARM or IRM) to compensate for variations in the concentration of remanence carrying grains. The chosen normalizer should activate the same grain population that carries the NRM. Susceptibility (κ) is sensitive to large multidomain (MD) grains and small (superparamagnetic, SP) grains which are either not important remanence carriers (in the case of MD grains) or not able to carry remanence (in the case of SP grains). ARM and IRM activate remanence carrying fine-grained magnetite. The mean grain size of the population of magnetite grains activated by IRM might be expected to be larger than for grains activated by ARM.

In figure 9, we plot NRM/κ, NRM/ARM and NRM/IRM for five demagnetization steps in the 25–45 mT range. Note that the value of the ratio is determined for a particular peak demagnetization field applied to NRM, and ARM or IRM. The variability of normalized remanence is similar for each normalizer (figure 9). Surprisingly, the NRM/ARM values are more variable than the NRM/κ or NRM/IRM values (figure 9). It appears that the NRM/ARM record is under normalized and that the coercivity spectra of NRM and ARM are more dissimilar than the coercivity spectra of NRM and IRM. For this reason, we chose NRM/IRM as the palaeointen-

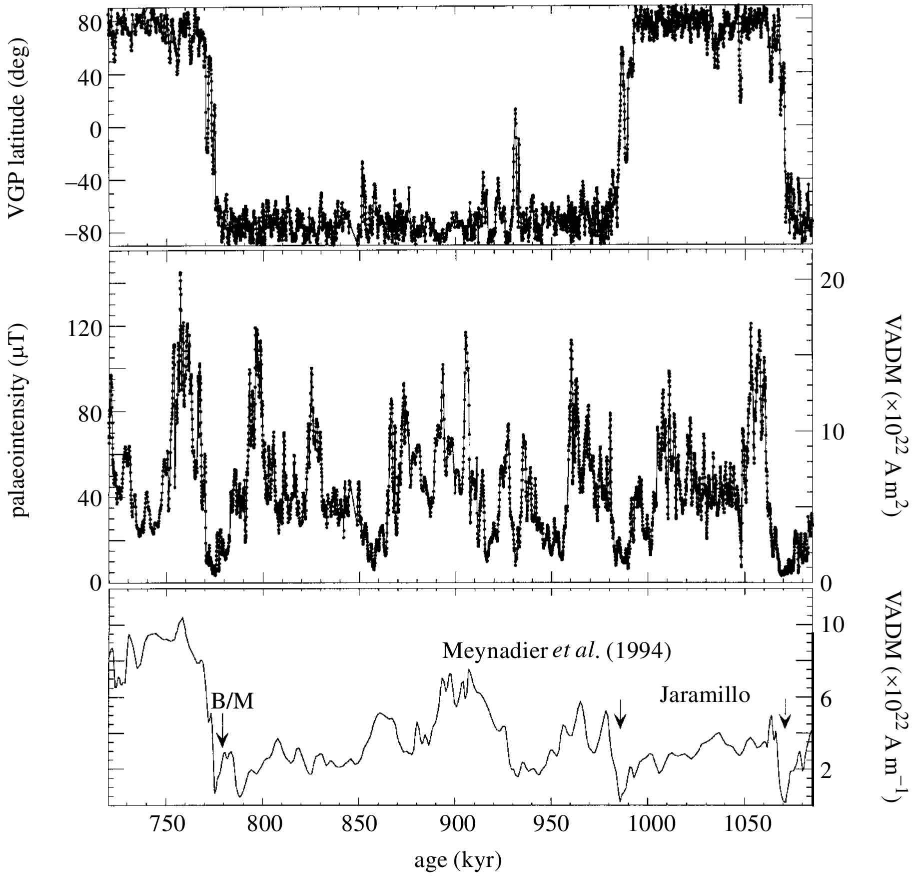

Figure 10. Site 983 virtual geomagnetic polar (VGP) latitudes computed from magnetization components (figure 8), mean NRM/IRM scaled to μT and represented as virtual axial dipole moment (VADM), and normalized remanence (paleointensity record) from ODP Hole 851D (Meynadier *et al.* 1994). Bathymetry in metres.

sity proxy. The arithmetic mean of the five values of NRM/IRM (for the 25–45 mT demagnetization range) provides the palaeointensity proxy.

Constable & Tauxe (1996) suggested a means of scaling sedimentary relative palaeointensity records using the assumption that the axial dipole (g_1^0) goes to zero at the time of reversal and that field intensity at that time is due to the non-axial-dipole field (NAD). They use an estimate of 7.5 μT for the strength of the NAD, then multiply the sedimentary palaeointensity record by a constant factor which sets the average transitional palaeointensity to 7.5 μT. The resulting scaled palaeointensity record for Site 983 is shown in figure 10. The average palaeointensity over the scaled record is 47.5 μT, which is comparable with the expected mean dipole field intensity at the site latitude (54.2 μT). The average virtual axial dipole moment (VADM) over the record is 6.8×10^{22} A m^2 with values falling to *ca.* 1×10^{22} A m^2 at polarity reversals (figure 10).

The MBB and the boundaries of the Jaramillo Subchronozone occur within palaeointensity lows, as do several intervals of high-amplitude secular variation (figure 10).

The palaeointensity low at about 793 ka that predates the directional change at the MBB (figure 10) appears to be the same as the pre-reversal palaeointensity low recorded in equatorial Pacific and North Atlantic cores (Kent & Schneider 1995; Hartl & Tauxe 1996). Other palaeointensity records for the Late Matuyama Chron are from the Pacific and Indian Oceans (Meynadier *et al*. 1994) and from Core K78030 from the central equatorial Pacific (Laj *et al*. 1996; Verosub *et al*. 1996). All these records are from piston cores with mean sedimentation rates of a few (1–3) cm kyr^{-1} in contrast to mean sedimentation rates of *ca.* 13 cm kyr^{-1} in this interval at Site 983 (see figure 4). Although the records of Meynadier *et al*. (1994) can be correlated from the Indian Ocean to the Pacific Oceans (see also Valet & Meynadier 1998), these records cannot be clearly correlated in detail to those from Core K78030, and none of these low resolution palaeointensity records can be correlated in detail to Site 983. An example of these correlation problems is shown in figure 10, where the record from central equatorial Pacific ODP Hole 851D (Meynadier *et al*. 1994) is shown with the Site 983 record. The progressive decrease in palaeointensity within the Jaramillo Subchronozone in the Meynadier *et al*. (1994) record was contributing evidence to the 'sawtooth' hypothesis of palaeointensity in which geomagnetic palaeointensity was thought to decrease within polarity chrons until critically low values triggered the polarity reversal process. The hypothesis continues to be the focus of debate, however, records showing this progressive decay in palaeointensity can, according to some authors, be explained by delayed remanence acquisition (see Mazaud 1996; Kok & Tauxe 1996; Meynadier *et al*. 1998). Recently, Valet *et al*. (1999) have made the case, based in absolute palaeointensity determinations from the Canary Islands, that the interval between the top of the Jaramillo and the MBB is characterized by an 'overall tendency' of the field to decrease. It is important to note that no clear overall decay of palaeointensity is apparent within the Jaramillo Subchronozone or between the Jaramillo Subchronozone and the MBB at Site 983 (figure 10).

7. Ages of polarity reversals

Since 1990, the ages of Late Miocene to Pleistocene polarity reversals have been revised due to astrochronological estimates from Italian land sections (e.g. Hilgen 1991*a*, *b*), from ODP Site 677 (Shackleton *et al*. 1990) and from ODP Leg 138 (Shackleton *et al*. 1995). These new ages are systematically older than the previously accepted ages (e.g. Berggren *et al*. 1985), which followed the K–Ar chronology of Mankinen & Dalrymple (1979). The generally accepted astrochronological ages for the MBB and the boundaries of the Jaramillo Subchron (Shackleton *et al*. 1990) are indicated in figure 11 together with the Site 983 virtual geomagnetic polar (VGP) latitudes placed on the $\delta^{18}O$ age model.

The duration of the polarity reversals, as determined by the length of time for which the VGP latitudes are less than 45°, is *ca.* 5 kyr for each reversal (figure 11). This estimate is comparable with the magnetic diffusion time of the Earth's inner core, estimated to be *ca.* 3 kyr, and is consistent with the idea that diffusion through the inner core is necessary to stabilize the reversing field (see Gubbins 1999).

For the *base* of the Jaramillo Subchronozone, the Site 983 estimate (figure 11) is consistent with the generally accepted astrochronological estimate (1070 ka) (Shackleton *et al*. 1990). Singer *et al*. (1999) gave $^{40}Ar/^{39}Ar$ ages from lavas recording the Jaramillo Subchron in the Punaruu Valley, Tahiti. Their age for the base of

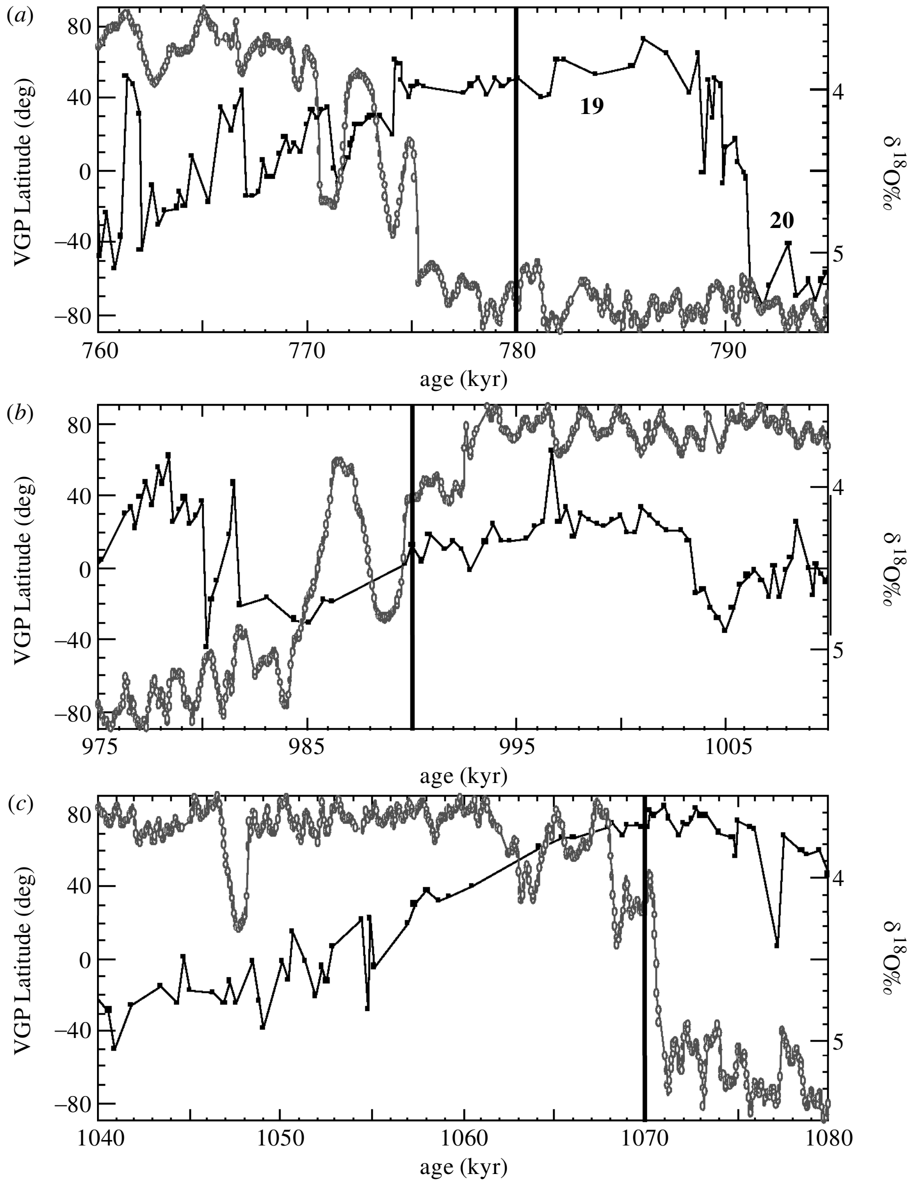

Figure 11. Virtual geomagnetic polar (VGP) latitudes (open symbols) and benthic δ^{18}O record (solid symbols) across (*a*) the Matuyama–Brunhes boundary (MBB) and (*b*), (*c*) the boundaries of the Jaramillo Subchronozone. Bold lettering indicates isotopic stage numbers. Thick vertical lines indicate the generally accepted astrochronological ages for these polarity chron boundaries (Shackleton *et al.* 1990).

the Jaramillo Subchronozone (1053 ± 6 ka) is midway between the earlier ^{40}Ar/^{39}Ar determinations of Spell & MacDougall (1992) and Izett & Obradovich (1994). For the *top* of the Jaramillo Subchronozone, the Site 983 estimate (figure 11) is again close to the generally accepted astrochronological estimate (990 ka) (Shackleton *et* *al*. 1990). The ^{40}Ar/^{39}Ar age given by Singer *et al*. (1999) (986 ± 5 ka) is consistent with these estimates. The process of checking astrochronological age estimates for reversal boundaries using ^{40}Ar/^{39}Ar methods is somewhat circular because the best way of calibrating the ^{40}Ar/^{39}Ar standards is by matching the ^{40}Ar/^{39}Ar and astrochronological estimates (see Renné *et al*. 1994).

The age of *onset* of the Matuyama–Brunhes reversal at Site 983 (775 ka) and the midpoint of the reversal (772.5 ka) (figure 11) are younger than the mean ^{40}Ar/^{39}Ar age of 778.7±1.9 ka given by Singer & Pringle (1996). The apparent age for the MBB from Site 983 is also younger than the generally accepted astrochronological estimate (780 ka) (Shackleton *et al*. 1990), and the estimate (778.0 ± 1.7 ka) by Tauxe *et al*. (1996) based on 19 oxygen isotope/magnetic records combined with the ^{40}Ar/^{39}Ar estimate of Singer & Pringle (1996). At Site 983, the MBB occurs at the young end of the isotopic stage 19 (compare figure 11 with fig. 3 of Tauxe *et al*. (1996)). The sedimentary sections where the MBB ages have been determined by astrochronology (e.g. ODP Sites 677 and DSDP Site 607) have lower sedimentation rates than Site 983. Note that ODP Site 677 does not have a polarity stratigraphy and the age of reversals was deduced by correlation to DSDP Hole 552A and DSDP Site 607 (Shackleton *et al*. 1990). The younger apparent age of the MBB at Site 983 could be attributed to the sedimentary record of polarity reversals being shifted down-section by a finite lock-in depth for magnetic remanence acquisition. The resulting time delay of remanence acquisition might be greater for lower sedimentation rates, as the lock-in depth would have greater temporal significance than in a higher sedimentation rate sequence (such as Site 983). This possible explanation for the relatively young age for the MBB at Site 983 is inconsistent with the findings of Tauxe *et al*. (1996), who concluded that the isotope-based (astrochronological) ages for the MBB do not show any systematic variation with sedimentation rate, implying shallow (few cm) magnetization lock-in depths.

For the Brunhes Chron (0–725 ka interval) at Site 983, Channell *et al*. (1998) documented *ca*. 100 kyr and *ca*. 41 kyr power in the NRM/IRM record and suggested that the 41 kyr power may be due to the geomagnetic field itself (see also Yamazaki 1999). The rationale for this conclusion was that no significant 41 kyr power was seen in the magnetic concentration parameters such as IRM, which would be expected to be sensitive to lithologic/climatic variability. In these Brunhes records, 100 kyr power was found to be ubiquitous in all magnetic concentration parameters (including IRM) reflecting the strong influence of the *ca*. 100 kyr orbital period on climate/lithology during this time.

Spectral analysis of the mean NRM/IRM record for the 700–1100 ka interval from Site 983 indicates power peaks at periods close to 41 kyr (0.0244 kyr^{-1}) and just greater than 100 kyr (0.01 kyr^{-1}) (figure 12). The power spectrum for IRM features a broad power peak close to 41 kyr. It is interesting to note the absence of 100 kyr power in IRM, presumably reflecting the diminished influence of this period on climate at this time (in the so-called 41 kyr world) relative to its strong influence in the Brunhes. The squared coherency between NRM/IRM and IRM is not significant at periods greater than *ca*. 12 kyr (figure 12) implying that the 41 kyr power in NRM/IRM is not be due to climatic influence on the palaeointensity record (through IRM) but rather to the geomagnetic field itself. The *ca*. 100 kyr power in NRM/IRM is also, in the records documented here, not easily attributed to climate/lithology as it is absent in IRM, and therefore, may also be attributed to the geomagnetic field.

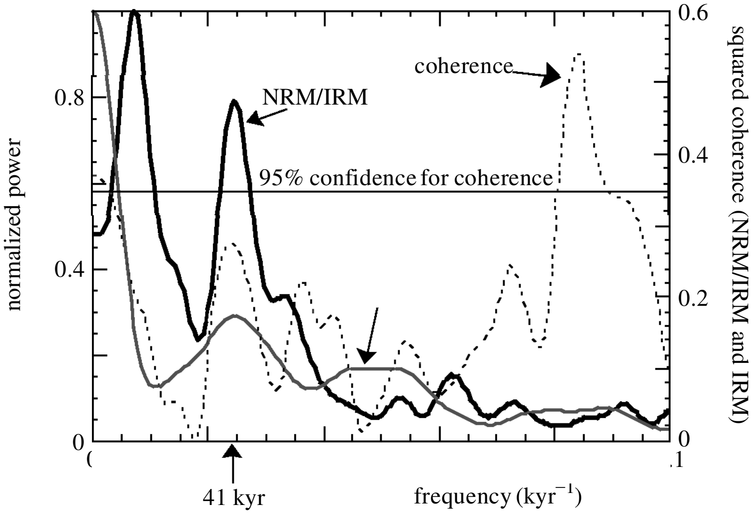

Figure 12. Power spectra using the Blackman–Tukey method with a Bartlett window for NRM/IRM (black continuous line) and $IRM_{35\ mT}$ (grey continuous line) in the 700–1100 ka interval at Site 983. Squared coherence between NRM/IRM and IRM (dashed line) indicating insignificant coherence at frequencies less than 0.08 kyr^{-1}.

We thank N. J. Shackleton and D. A. Hodell for mass spectrometry support and advice concerning the age model during research stays (H.F.K.) at University of Cambridge and University of Florida. We are very grateful to E. Jansen, C. Laj, C. Kissel and A. Mazaud for logistical support and scientific advice. C. Laj, B. Clement and N. J. Shackleton provided helpful comments on the manuscript. This work was supported by NSF grant EAR 98-04711, the US Science Support Program for ODP Leg 162 and by the Norwegian Research Council.

References

Bassinot, F., Labeyrie, L., Vincent, E., Quidelleur, X., Shackleton, N. J. & Lancelot, Y. 1994 The astronomical theory of climate and the age of the Brunhes–Matuyama boundary. *Earth Planet. Sci. Lett.* **126**, 91–108.

Berger, A. & Loutre, M. F. 1991 Insolation values for the climate of the last 10 million years. *Quat. Sci. Rev.* **10**, 297–317.

Berggren, W. A., Kent, D. V. & van Couvering, J. A. 1985 The Neogene. Part 2. Neogene geochronology and chronostratigraphy. In *Chronology of the geological record* (ed. N. J. Snelling), pp. 211–260. Blackwell Scientific Publications, Oxford Press.

Bickert, T., Curry, W. B. & Wefer, G. 1997 Late Pliocene to Holocene (2.6–0 Ma) western equatorial Atlantic deep-water circulation: inferences from benthic stable isotopes. In *Proceedings of the Ocean Drilling Program, Scientific Results*, vol. 154, pp. 239–254. College Station, TX: Ocean Drilling Program.

Channell, J. E. T. & Lehman, B. 1999 Magnetic stratigraphy of Leg 162 North Atlantic Sites 980–984. In *Proceedings of the Ocean Drilling Program, Scientific Results*, vol. 162, pp. 113–130. College Station, TX: Ocean Drilling Program.

Channell, J. E. T., Hodell, D. A. & Lehman, B. 1997 Relative geomagnetic paleointensity and $\delta^{18}O$ at ODP Site 983 (Gardar Drift, North Atlantic) since 350 ka. *Earth Planet. Sci. Lett.* **153**, 103–118.

Channell, J. E. T., Hodell, D. A., McManus, J. & Lehman, B. 1998 Orbital modulation of geomagnetic paleointensity. *Nature* **394**, 464–468.

Constable, C. & Tauxe, L. 1996 Towards absolute calibration of sedimentary paleointensity records. *Earth Planet. Sci. Lett.* **143**, 269–274.

Day, R., Fuller, M. & Schmidt, V. A. 1977 Hysteresis properties of titanomagnetites: grain-size and compositional dependence. *Phys. Earth Planet. Interiors* **13**, 260–267.

Dokken, T. M. & Jansen, E. 1999 Rapid changes in the mode of deep—and intermediate water formation during the last glacial. *Nature* **401**, 458–461.

Gubbins, D. 1999 The distinction between geomagnetic excursions and reversals. *Geophys. J. Int.* **137**, F1–F3.

Hagelberg, T., Shackleton, N. J., Pisias, N. & Shipboard Scientific Party 1992 Development of composite depth sections for Sites 844 through 854. In *Proceedings of the Ocean Drilling Program, Scientific Results*, vol. 138, pp. 79–85. College Station, TX: Ocean Drilling Program.

Hartl, P. & Tauxe, L. 1996 A precursor to the Matuyama/Brunhes transition-field instability as recorded in pelagic sediments. *Earth Planet. Sci. Lett.* **138**, 121–135.

Hilgen, F. J. 1991*a* Astronomical calibration of Gauss to Matuyama Sapropels in the Mediterranean and implication for the geomagnetic polarity time scale. *Earth Planet. Sci. Lett.* **104**, 226–244.

Hilgen, F. J. 1991*b* Extension of the astronomically calibrated (polarity) time scale to the Miocene/Pliocene boundary. *Earth Planet. Sci. Lett.* **107**, 349–368.

Imbrie, J. & Imbrie, J. Z. 1980 Modeling the climatic response to orbital variations. *Science* **207**, 943–953.

Izett, G. A. & Obradovich, J. D. 1994 $^{40}Ar/^{39}Ar$ age constraints for the Jaramillo Normal Subchron and the Matuyama–Brunhes geomagnetic boundary. *J. Geophys. Res.* **99**, 2925–2934.

Kent, D. V. & Schneider, D. A. 1995 Correlation of paleointensity variation records in the Brunhes/Matuyama polarity transition interval. *Earth Planet. Sci. Lett.* **129**, 135–144.

King, J. W., Banerjee, S. K. & Marvin, J. 1983 A new rock-magnetic approach to selecting sediments for geomagnetic paleointensity studies: application to paleointensity for the last 4000 years. *J. Geophys. Res.* **88**, 5911–5921.

Kirschvink, J. L. 1980 The least squares lines and plane analysis of paleomagnetic data. *Geophys. J. R. Astr. Soc.* **62**, 699–718.

Kok, Y. S. & Tauxe, L. 1996 Saw-toothed pattern of sedimentary paleointensity records explained by cumulative viscous remanence. *Earth Planet. Sci. Lett.* **137**, 95–99.

Laj, C., Kissel, C. & Garnier, F. 1996 Relative geomagnetic field intensity and reversals for the last 1.8 My from a central Pacific core. *Geophys. Res. Lett.* **23**, 3393–3396.

McCave, I. N. & Tucholke, B. E. 1986 Deep current-controlled sedimentation in the western North Atlantic. In *The geology of North America*, vol M: *The western North Atlantic region* (ed. P. R. Vogt & B. E. Tucholke), pp. 451–468. Boulder, CO: Geological Society of America.

McCave, I. N., Lonsdale, P. F., Hollister, C. D. & Gardner, W. D. 1980 Sediment transport over the Hatton and Gardar contourite drifts. *J. Sediment. Pet.* **50**, 1049–1062.

McManus, J., Oppo, D. W. & Cullen, J. L. 1999 A 0.5-million-year record of millennial-scale climate variability in the North Atlantic. *Science* **283**, 971–974.

Mankinen, E. A. & Dalrymple, G. B. 1979 Revised geomagnetic polarity time scale for the interval 0–5 m.y.b.p. *J. Geophys. Res.* **84**, 615–626.

Manley, P. L. & Caress, D. W. 1994 Mudwaves on the Gardar Sediment Drift, NE Atlantic. *Paleoceanography* **9**, 973–988.

Martinson, D. G., Pisias, N. G., Hays, J. D., Imbrie, J., Moore Jr, T. C. & Shackleton, N. J. 1987 Age dating and the orbital theory of the Ice Ages: development of a high-resolution 0 to 300,000-year chronostratigraphy. *Quat. Res.* **27**, 1–29.

Mazaud, A. 1996 'Saw-tooth' variation in magnetic intensity profiles and delayed acquisiton of the magnetization in deep sea sediments. *Earth Planet. Sci. Lett.* **139**, 379–386.

Meynadier, L., Valet, J.-P., Bassinot, C., Shackleton, N. J. & Guyodo, Y. 1994 Asymmetrical saw-tooth pattern of the geomagnetic field intensity from equatorial sediments in the Pacific and Indian Oceans. *Earth Planet. Sci. Lett.* **126**, 109–127.

Meynadier, L., Valet, J.-P., Guyodo, Y. & Richter, C. 1998 Saw-toothed variations of relative paleointensity and cumulative viscous remanence: testing the records and the model. *J. Geophys. Res.* **103**, 7095–7105.

Ortiz, J., Mix, A., Harris, S. & O'Connell, S. 1999 Diffuse spectral reflectance as a proxy for percent carbonate content in North Atlantic sediments. *Paleoceanography* **14**, 171–186.

Raymo, M. E., Ganley, K., Carter, S., Oppo, D. W. & McManus, J. 1998 Millennial-scale climate instability during the early Pleistocene epoch. *Nature* **392**, 699–702.

Renné, P. R., Deino, P. L., Walter, R. C., Turrin, B. D., Swisher III, C. C., Becker, T. A., Curtis, G. H., Sharp, W. D. & Abdur-Rahim, J. 1994 Intercalibration of astronomical and radioisotopic time. *Geology* **22**, 783–786.

Ruddiman, W. F., Raymo, M. E., Martinson, D. G., Clement, B. M. & Backman, J. 1989 Pleistocene evolution: Northern Hemisphere ice sheets and north Atlantic Ocean. *Paleoceanography* **4**, 353–412.

Shackleton, N. J., Berger, A. & Peltier, W. R. 1990 An alternative astronomical calibration of the lower Pleistocene timescale based on ODP Site 677. *Trans. R. Soc. Edinb. Earth Sci.* **81**, 251–261.

Shackleton, N. J., Crowhurst, S., Hagelberg, T., Pisias, N. G. & Schneider, D. A. 1995 A new Late Neogene time scale: application to Leg 138 sites. In *Proceedings of the Ocean Drilling Program, Scientific Results*, vol. 138, pp. 73–104. College Station, TX: Ocean Drilling Program.

Shipboard Scientific Party, Site 983 1996 *Proceedings of the Ocean Drilling Program, Initial Reports*, vol. 162, pp. 139–167. College Station, TX: Ocean Drilling Program.

Singer, B. S. & Pringle, M. S. 1996 Age and duration odf the Matuyama–Brunhes geomagnetic polarity reversal from $^{40}Ar/^{39}Ar$ incremental heating analysis of lavas. *Earth Planet. Sci. Lett.* **139**, 47–61.

Singer, B. S., Hoffman, K. A., Chauvin, A., Coe, R. S. & Pringle, M. S. 1999 Dating transitionally magnetized lavas of the late Matuyama Chron: toward a new $^{40}Ar/^{39}Ar$ timescale of reversals and events. *J. Geophys. Res.* **104**, 679–693.

Spell, T. L. & McDougall, I. 1992 Revisions to the age of the Brunhes/Matuyama boundary and the Pleistocene geomagnetic polarity timescale. *Geophys. Res. Lett.* **19**, 1182–1184.

Tauxe, L. 1993 Sedimentary records of relative paleointensity of the geomagnetic field: theory and practice. *Rev. Geophys.* **31**, 319–354.

Tauxe, L., LaBrecque, J. L., Dodson, R. & Fuller, M. 1983 U-channels—a new technique for paleomagnetic analysis of hydraulic piston cores. *Eos* **64**, 219.

Tauxe, L., Herbert, T., Shackleton, N. J. & Kok, Y. S. 1996 Astronomical calibration of the Matuyama–Brunhes boundary: consequences for the magnetic remanence acquisition in marine carbonates and Asian loess sequences. *Earth Planet. Sci. Lett.* **140**, 133–146.

Tiedemann, R., Sarnthein, M. & Shackleton, N. J. 1994 Astronomic timescale for the Pliocene Atlantic $\delta^{18}O$ and dust flux records of Ocean Drilling Program Site 659. *Paleoceanography* **9**, 619–638.

Valet, J.-P. & Meynadier, L. 1998 A comparison of different techniques for relative paleointensity. *Geophys. Res. Lett.* **25**, 89–92.

Valet, J.-P., Brassart, J., Quidelleur, X., Soler, V., Gillot, P.-Y. & Hongre, L. 1999 Paleointensity variations across the last geomagnetic reversal at La Palma, Canary Islands, Spain. *J. Geophys. Res.* **104**, 7577–7598.

Verosub, K. L., Herrero-Bervera, E. & Roberts, A. P. 1996 Relative geomagnetic paleointensity across the Jaramillo subchron and the Matuyama/Brunhes boundary. *Geophys. Res. Lett.* **23**, 467–470.

PHILOSOPHICAL TRANSACTIONS OF THE ROYAL SOCIETY A MATHEMATICAL, PHYSICAL & ENGINEERING SCIENCES

Vidal, L., Labeyrie, L. & van Weering, T. C. E. 1998 Benthic δ^{18}O records in the North Atlantic over the last glacial period (60–10 kyr): evidence for brine formation. *Paleoceanography* **13**, 245–251.

Weeks, R., Laj, C., Endignoux, L., Fuller, M., Roberts, A., Manganne, R., Blanchard, E. & Goree, W. 1993 Improvements in long-core measurement techniques: applications in palaeomagnetism and palaeoceanography. *Geophys. J. Int.* **114**, 651–662.

Wold, C. N. 1994 Cenozoic sediment accumulation on drifts in the northern North Atlantic. *Paleoceanography* **9**, 917–941.

Yamazaki, T. 1999 Relative paleointensity of the geomagnetic field during the Brunhes Chron recorded in the North Pacific deep-sea sediment cores: orbital influence? *Earth Planet. Sci. Lett.* **169**, 23–35.